RVE Based Multilevel Method For Periodic Heterogeneous Media With Strong Scale Mixing

Jacob Fish and Wen Chen

Department of Mechanical, Aerospace and Nuclear Engineering,
Rensselaer Polytechnic Institute, Troy, NY 12180, USA

Abstract: Representative Volume Element based multilevel (multigrid) solution method for wave propagation problems in periodic heterogeneous media is developed. The intergrid transfer operators are constructed from the solution of the Representative Volume Element (RVE) problem. We show that the convergence of the RVE-based multilevel method improves with increasing material heterogeneity and decreasing time integration step. Numerical results confirm theoretical estimates.

Key Words: multilevel; heterogeneous medium; aggregation; rate of convergence; RVE;

1.0 Introduction

We focus on the class of problems for which the size of the microstructure is comparable in magnitude to that of structural details or the wavelength of a traveling signal. This class of problems falls into the grey area where the distinction between the structure and the material is not obvious at best. A number of important problems fall into this category including: (i) 3D woven architectures in aircraft engines [1][2], (ii) airframes, (iii) tires [3][4], (iv) micro-electronic devices [5], and (v) porous engineering materials such as honeycombs and truss-like materials [6]. Figure 1 depicts a typical 3D material architecture [7][8]. The size of the Representative Volume Element (RVE) in woven composites ranges from one quarter of inch to more than an inch. These large 3D material architectures are often used in
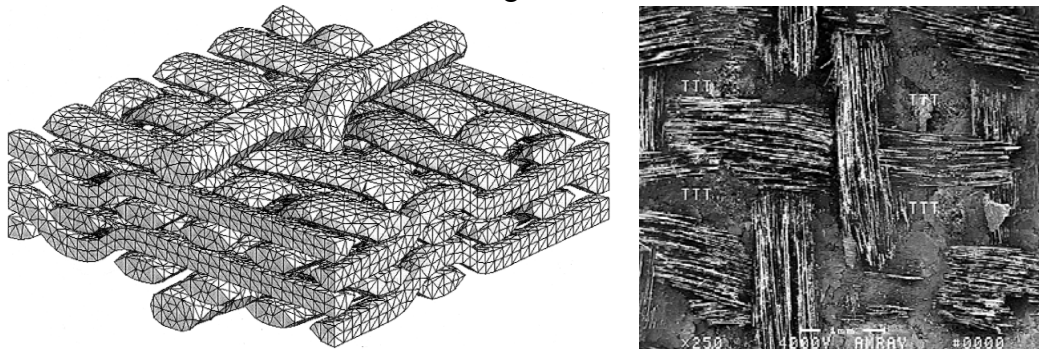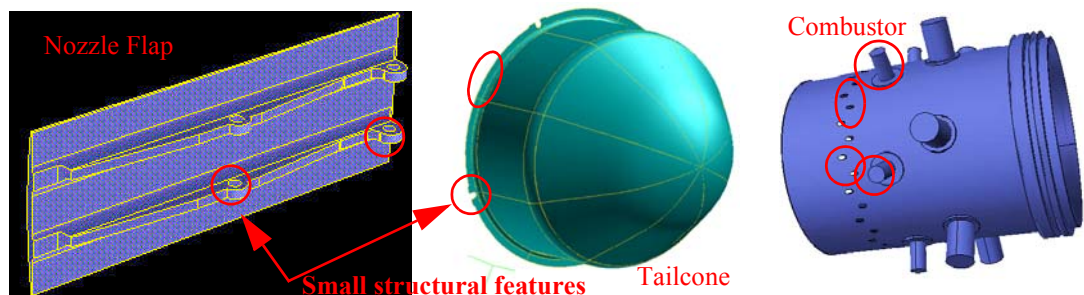

Figure 1: A typical 3D material architecture

Figure 2: Structural Components made of 3D woven composites

structural components where the structural details such as holes, cutouts and other interconnecting parts are of the same order of magnitude as that of the RVE. Three examples of such

a profound scale mixing are shown in Figure 2.

Tires represent another example where material and structural scales are inseparable. A single tire today contains more than 200 raw materials. It features a complex architecture of steel belts, textile plies and tread patterns, designed to produce optimal performance characteristics for each type of tire. Tires are made from rubber and cord/rubber 3D composite components as shown in Figure 3a. The tread and sidewall are all rubber, while the belts and plies are unidirectional lamina with continuous cords of polyester, rayon, or nylon fibers, or twisted steel wires. When the relatively stiff wires have cut ends surrounded by rubber, this creates a stress riser for the rubber and a natural location for damage, flaw initiation and growth [3][4]. Cord diameters could be up to 2 mm, which is of the same order of magnitude as the steel belt thickness.

Coupling of scales is even more profound in Multichip Modules (MCM) which are characterized by a number of layers containing wires and vias in various configurations, in conjunction with a general chip and cooling structure layout [5]. A typical multichip module is shown in Figure 3b. It can be seen that in MCM vias are of the same size as the structural details (single chip).
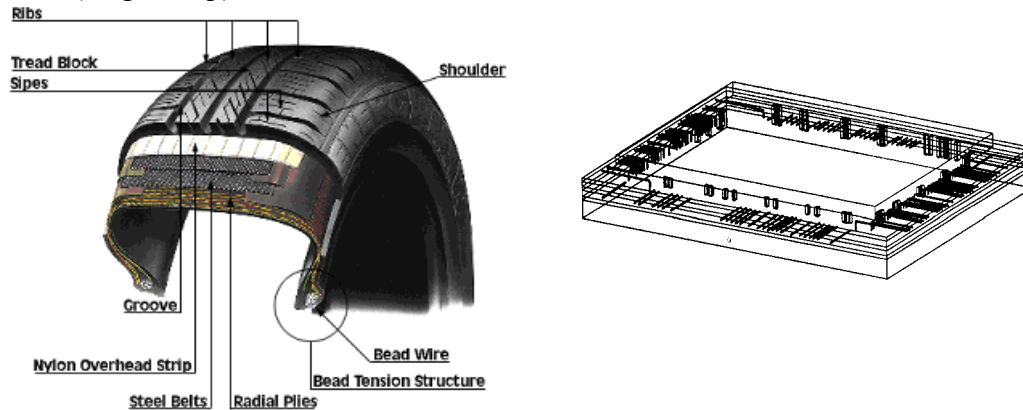

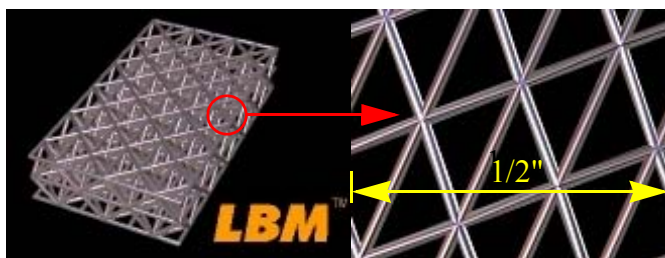Figure 3: (a) Tire Structure, (b) Single chip

Figure 4: Lattice Block Material

Finally, Figure 4 depicts an example of a Lattice Block Material developed by JAMCORP corporation [6]. It can be seen that the size of the RVE is approximately 12 inches resulting in strong scale coupling between the scales. Lattice Block Materials (LBM) are a family of structural materials that derive their mechanical performance from their structure of highly ordered internal tetrahedra. LBM may be manufactured in steel, aluminum, plastics, rubber or ceramics. LBM technology provides a nearly optimal strength-to-weight ratio.

Various multiscale solution approaches in the modern era can be classified into two categories: (a) multiple scale expansion methods ([15]-[21]), and (b) global-local methods ([22]-[32]). In what follows we briefly review the two approaches and their applicability to problems with strong scale mixing.

Multiple scale expansion methods have been employed by Ghosh [15][16], Herakovich

[17], Kikuchi [18], [19], Fish [13], [20], [21] and others. These methods hinge on the following three assumptions: (i) the macrostructure is formed by a spatial repetition of RVEs, (ii) solution is locally periodic, and (iii) macroscopic fields are constant within a single RVE. Typically these assumptions are valid away from the boundary layer regions and as long as the microstructure is significantly smaller than a typical dimension of the macrostructure or the wavelength of a traveling signal.

The hallmark of global-local techniques ([22]-[32]), is the ability to capitalize on the existence of relatively small region(s) within the problem domain requiring a refined mathematical/numerical modeling. Such approaches may not be adequate for problems with numerous interacting local effects which may dynamically evolve (transient problems).

In this paper we focus on problems with strong scale mixing for which existing methods are either inaccurate (multiple scale expansion methods) or computationally intractable (global-local methods). For this class of problems we propose to utilize a multilevel approach with special intergrid transfer operators constructed from the solution of the RVE problem. We will refer to such a method as the RVE-based multilevel method. For differential equations with oscillatory coefficients the classical multigrid approach with standard linear interpolation operators is not well suited to approximate the lower frequency response, mainly because the lower frequency eigenvectors are not smooth for problems in heterogeneous media. In statics, it has been shown [33][34] that the solution based on the homogenization theory represents exactly the lower frequency response of the source problem resulting in a rate of convergence of the two-level method governed by

$$\left\| e^{i+1} \right\|_2 = \gamma \left\| e^i \right\|_2, \quad \gamma = (1 + d + 1/d)^{-1} \tag{1}$$

provided that the middle frequency of the error can be filtered out. In Eqn (1) $e^i = u^i - u^{ex}$

where u^i, u^{ex} reprensent the solution at iteration i and the exact solution, respectively, and d is the ratio of microconstituents stiffness. Note that for homogeneous media, $d=1$, discretized with a uniform finite element mesh the classical multigrid estimate, stating that asymptotically the error reduces by a factor of three with each cycle, is recovered. On the other hand if one micro-phase is significantly stiffer than the other, i.e. $d \gg 1$ or $d \ll 1$, the two-level method converges in a single cycle.
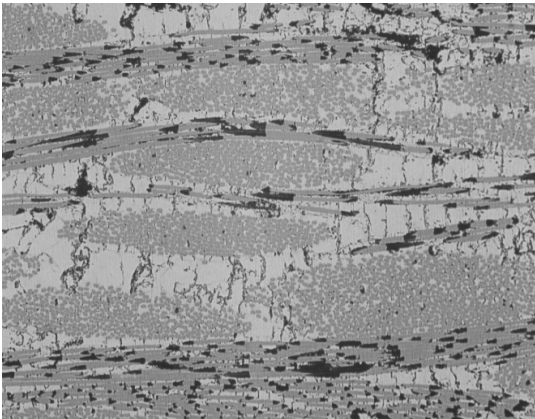
Figure 5: Cracking in Blackglass matrix problems.

Tires, multichip modules (MCMs) and woven ceramic composites fall into the category of problems for which $d \gg 1$ or $d \ll 1$. Cord-rubber stiffness ratio is about 1000/1 in the axial direction [3]; bundle-matrix stiffness ratio in high temperature woven composites is over 100/1 due to excessive cracking in the matrix domain resulting from material processing [1] (Figure 5); copper-polyimide stiffness ratio is about 50/1 in MCMs, while thermal conductivity ratio is over 1000/1 [5]. The two-level method [33][34] is ideally suited for this type of

The primary objective of the present manuscript is to extend the methodology developed in [33][34] to transient problems. We show that for transient problems the homogenized model does not capture the lower frequency response of the source problem. A nearly optimal prolongation operator can be constructed from the solution of the equivalent static problem on the RVE domain. The mid-frequency errors, which are often unaffected by the smoother and coarse model correction [33], can be filtered out using a three-level approach based on the global-basis multilevel method [35][36].

We focus on a special class of multilevel methods for a symmetric positive definite system of equations

$$Ku = f \qquad u \in \Re^n, f \in \Re^n, K \in \Re^{n \times n} \tag{2}$$

arising from the discretization in space and time of the initial-boundary value problem describing the wave propagation in heterogeneous media. The following notation is employed throughout the paper. We define the prolongation operator, Q, as $Q : \Re^m \to \Re^n$. The restriction operator, Q^T, from the fine to coarse model is the transpose of the prolongation operator $Q^T : \Re^n \to \Re^m$. The coarse model matrix K_0 is the restriction of K:

$$K_0 = Q^T K Q \qquad K_0 \in \Re^{m \times m} \tag{3}$$

The smoothing preconditioner and coarse model preconditioner are denoted as $P \in \Re^{n \times n}$ and $C = (Q K_0^{-1} Q^T)^{-1} \in \Re^{n \times n}$, respectively. The smoothing and coarse model correction iteration matrices are denoted as $S = I - P^{-1} K \in \Re^{n \times n}$ and $T = I - C^{-1} K \in \Re^{n \times n}$, respectively, where I is the $n \times n$ identity matrix. The error reduction, $e^{i+1} = L e^i$, in a complete two-level cycle is governed by a two-level iteration matrix

$$L = R^v T R^v \in \Re^{n \times n} \tag{4}$$

with v post- and pre- smoothing iterations. For more details we refer to [37]-[41].

Except for a small fraction of mid-frequency eigenmodes, most of the eigenvalues of the stiffness matrix (2) are clustered at the two ends of the spectrum [33][34]. While low and high frequency modes of error can be efficiently captured by the coarse model and smoother, respectively, the mid-range frequencies can be eliminated using global-basis multilevel method [35][36]. By this approach the mid-range frequencies of error are filtered out by introducing an additional coarse level with a prolongation operator, $q : \Re^k \to \Re^n$, spanning the subspace defined by a linear combination of k eigenvectors corresponding to the largest eigenvalues of L. The resulting three level iteration matrix, $\hat{L}$, is given as

$$\hat{L} = L[I - q(q^T K q)^{-1} q^T K] L \in \Re^{n \times n} \tag{5}$$

2.0 Convergence Analysis for 1D Model Problem

For convergence studies we consider the following elastodynamics model problem with some initial and Dirichlet boundary conditions

$$\rho(x/\varepsilon)\ddot{u} - [E(x/\varepsilon)u_{,x}]_{,x} = 0, \quad u(x, 0) = F(x), \quad \dot{u}(x, 0) = 0$$
$$u(0, t) = 0, u(l, t) = 0 \tag{6}$$

where $u(x, t)$ denotes the displacement field; $\rho(x/\varepsilon)$ and $E(x/\varepsilon)$ are the mass density and elastic modulus of the medium, respectively; $0 < \varepsilon \ll 1$ is a small parameter denoting rapid spatial variation of material properties. The problem domain $\Omega(0, l)$ consists of a heterogeneous medium formed by a spatial repetition of the RVE composed of two materials phases as shown in Figure 6. Each RVE is discretized with two elements, one element for each material phase.
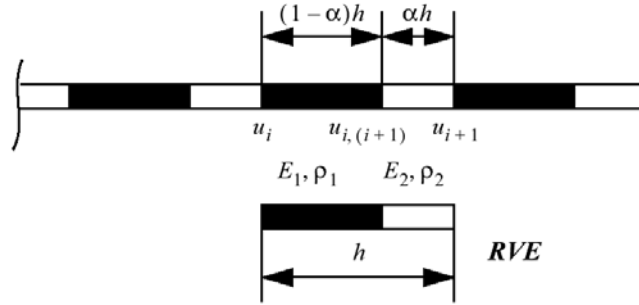
Figure 6: Model problem definition

It has been shown that in statics [33][34], the optimal coarse model can be constructed from the boundary value problem with constant (averaged) material properties given by

$$E_0 = \frac{E_1 E_2}{\alpha E_1 + (1 - \alpha)E_2}, \quad \rho_0 = (1 - \alpha)\rho_1 + \alpha\rho_2 \tag{7}$$

where E_1, E_2, ρ_1 and ρ_2 are the elastic moduli and mass density of the two constituent material phases, respectively; α is the volume fraction of the RVE constituent denoted by subscript *2*. For dynamics, however, this approach has been found to be inefficient, in particular when the equivalent stiffness matrix resulting from the Newmark integration scheme is dominated by the mass matrix (see Eqn. (8)). Construction of a nearly optimal coarse model for dynamics and analysis of the resulting two-level iterative process are the subjects of sections 2.1 and 2.2.

2.1 Convergence of the RVE based two-level method

We consider a coarse grid whose nodes coincide with the RVE boundaries as shown in Figure 6. The number of nodes in the coarse grid is m; the number of RVEs is $m - 1$ and the number of nodes in the source grid is $n = 2m - 1$. The coarse and the source grid dis-

placements are denoted by $\hat{\boldsymbol{u}}$ and $\boldsymbol{u}$, respectively. In the source grid, nodal displacements at the RVE boundaries are denoted by u_i, $i = 1, 2, \ldots, m$; nodal displacements inside the RVE are denoted by $u_{i,(i+1)}$, $i = 1, 2, \ldots, m-1$.

2.1.1 The RVE based two-level prolongation operator

For the two-element RVE the equivalent stiffness matrix is given as

$$\bar{\boldsymbol{K}}_a = \boldsymbol{K}_a + \frac{1}{\beta \Delta t^2} \boldsymbol{M}_a = \begin{bmatrix} a + cm_1/m_0 & -a & 0 \\ -a & a+b+c & -b \\ 0 & -b & b + cm_2/m_0 \end{bmatrix} \tag{8}$$

where β is the parameter in the Newmark scheme and Δt is the time step size; $\boldsymbol{K}_a$ and $\boldsymbol{M}_a$ are the assembled RVE stiffness and lumped mass matrices; $m_1 = (1-\alpha)h\rho_1 A$ and $m_2 = \alpha h \rho_2 A$ are the masses of the two constituent phases and $m_0 = m_1 + m_2 = \rho_0 hA$ is the total mass of the RVE; A and h are the cross-sectional area and the length of the RVE, respectively; and

$$a = \frac{K_1}{(1-\alpha)h}, \quad b = \frac{K_2}{\alpha h}, \quad c = \frac{m_0}{2\beta \Delta t^2}, \quad K_1 = E_1 A, \quad K_2 = E_2 A \tag{9}$$

The construction of the prolongation operator is based on the minimization of the RVE strain energy

$$\Pi_a = \frac{1}{2}\bar{\boldsymbol{u}}^T \bar{\boldsymbol{K}}_a \bar{\boldsymbol{u}} \tag{10}$$

subjected to the displacement compatibility condition between the adjacent RVEs:

$$\begin{bmatrix} 1 & 0 \\ \theta & \delta \\ 0 & 1 \end{bmatrix} \begin{bmatrix} \hat{u}_i \\ \hat{u}_{i+1} \end{bmatrix} = \begin{bmatrix} u_i \\ u_{i,(i+1)} \\ u_{i+1} \end{bmatrix}, \quad i = 1, 2, \ldots, m-1 \tag{11}$$

where $\bar{\boldsymbol{u}} = \begin{bmatrix} u_i & u_{i,(i+1)} & u_{i+1} \end{bmatrix}^T$. The solution of the constrained minimization problem yields

$$\theta = \frac{a}{a+b+c}, \quad \delta = \frac{b}{a+b+c} \tag{12}$$

For static case, $c = 0$, with homogeneous material properties and the volume fraction $\alpha = 0.5$, the interpolation parameters in (12) reduce to $\theta = \delta = 0.5$, which corresponds to the classical linear interpolants.

The global prolongation operator Q is formed by assembling the prolongation matrices of RVEs

$$
Q = \begin{bmatrix}
1 & & \\
\theta & \delta & \\
& 1 & \\
& \theta & \delta \\
& \cdots & \cdots & \cdots & \cdots \\
& & & \theta & \delta \\
& & & & 1
\end{bmatrix}_{n \times m}
\tag{13}
$$

Using lumped mass matrix formulation, the global equivalent stiffness matrix of the source grid has a tridiagonal form

$$
\bar{K} = \begin{bmatrix}
a+b+c & -b & & & & \\
-b & a+b+c & -a & & & \\
& -a & a+b+c & -b & & \\
& \cdots & \cdots & \cdots & \cdots & \cdots \\
& & & -a & a+b+c & -b \\
& & & & -b & a+b+c
\end{bmatrix}_{(n-2) \times (n-2)}
\tag{14}
$$

The coarse model equivalent stiffness matrix, obtained by the restriction of the source grid matrix, $\bar{K}_0 = Q^T \bar{K} Q$, is also a tridiagonal matrix

$$
\bar{K}_0 = g \ \text{tridiag}\{-1, 2, -1\} + f I
\tag{15}
$$

where

$$
g = \delta a + \theta b - \delta \theta (a+b+c), \quad f = (a+b)(\theta + \delta - 1)^2 + c[(\theta + \delta)^2 + 1]
\tag{16}
$$

2.1.2 Eigenpairs of the equivalent stiffness matrices

We first relate the eigenpairs of the source grid equivalent stiffness $\bar{K}$ to those of the coarse model equivalent stiffness matrix $\bar{K}_0$. We note that if $\hat{\phi}$ is an eigenvector of $\bar{K}_{01} = g \ \text{tridiag}\{-1, 2, -1\}$, it is also an eigenvector of $\bar{K}_0$, i.e.,

$$
\bar{K}_{01} \hat{\phi} = \hat{\lambda}_1 \hat{\phi}, \quad \bar{K}_0 \hat{\phi} = \hat{\lambda} \hat{\phi}
\tag{17}
$$

and the eigenvalues are related by

$$\hat{\lambda} = \hat{\lambda}_1 + f \tag{18}$$

The eigenvectors of $\overline{K}_{01}$ are (c.f. Hackbusch [38])

$$\hat{\phi}_i^k = \sin\frac{(i-1)k\pi}{m-1}, \quad 1 \le i \le m, \quad 1 \le k \le m-2 \tag{19}$$

where the superscript represents the eigenvector number and the subscript denotes the components of a specific eigenvector.

The first equation in (17) can be written as

$$g(-\hat{\phi}_{i-1}^k + 2\hat{\phi}_i^k - \hat{\phi}_{i+1}^k) = \hat{\lambda}_1^k \hat{\phi}_i^k, \quad 2 \le i \le m-1 \tag{20}$$

Substituting the eigenvectors in (19) into (20) yields

$$\hat{\lambda}_1^k = 4g\left[\sin\frac{k\pi}{2(m-1)}\right]^2, \quad \hat{\lambda}^k = 4g\left[\sin\frac{k\pi}{2(m-1)}\right]^2 + f, \quad 1 \le k \le m-2 \tag{21}$$

The eigenvalue problem of the source grid is

$$\overline{K}\phi^p = \lambda^p \phi^p, \quad 1 \le p \le n-2 \tag{22}$$

which in view of Eqn (14) can be written as

$$-a\phi_i^p + (a+b+c)\phi_{i,(i+1)}^p - b\phi_{i+1}^p = \lambda^p \phi_{i,(i+1)}^p, \quad 1 \le i \le m-1$$

$$-b\phi_{(i-1),i}^p + (a+b+c)\phi_i^p - a\phi_{i,(i+1)}^p = \lambda^p \phi_i^p, \quad 2 \le i \le m-1$$

$$\phi_1^p = 0, \quad \phi_m^p = 0, \quad 1 \le p \le n-2 \tag{23}$$

We denote the prolongation of the eigenvector $\hat{\phi}^k$ into the interior node of the RVE as $\hat{\phi}_{i,(i+1)}^k$ and it is prolongated in accordance with the prolongation matrix of the RVE (11), i.e.,

$$\hat{\phi}_{i,(i+1)}^k = \theta\hat{\phi}_i^k + \delta\hat{\phi}_{i+1}^k \tag{24}$$

We first solve for the $m-2$ smallest eigenpairs (λ^k, ϕ^k), where $1 \le k \le m-2$. We assume that the eigenvectors on the source grid are related to the eigenvectors on the coarse model by

$$\phi_i^k = \hat{\phi}_i^k, \quad 1 \le i \le m$$

$$\phi_{i,(i+1)}^k = w^k \hat{\phi}_{i,(i+1)}^k, \quad 1 \le i \le m-1, \quad 1 \le k \le m-2 \tag{25}$$

where w^k are parameters to be determined. Substituting (25) into (23) yields

$$(a+b+c)w^k \hat{\phi}_{i,(i+1)}^k - a\hat{\phi}_i^k - b\hat{\phi}_{i+1}^k = \lambda^k w^k \hat{\phi}_{i,(i+1)}^k, \quad 1 \le i \le m-1$$

$$(a+b+c)\hat{\phi}_i^k - aw^k \hat{\phi}_{i,(i+1)}^k - bw^k \hat{\phi}_{(i-1),i}^k = \lambda^k \hat{\phi}_i^k, \quad 2 \le i \le m-1$$

$$\hat{\phi}_1^k = 0, \quad \hat{\phi}_m^k = 0, \quad 1 \le k \le m-2 \tag{26}$$

Inserting Eqns (12) and (24) into (26) and using the relation (20) for the eigenpairs of the coarse model, we have

$$(w^k - 1)\hat{\phi}_{i,(i+1)}^k = \frac{w^k \lambda^k}{s} \hat{\phi}_{i,(i+1)}^k, \quad 1 \le i \le m-1$$

$$\left\{ s + \left[\frac{ab}{s}\left(\frac{\hat{\lambda}_1^k}{g} - 2\right) - \frac{a^2+b^2}{s} \right] w^k \right\} \hat{\phi}_i^k = \lambda^k \hat{\phi}_i^k, \quad 1 \le i \le m$$

$$\hat{\phi}_1^k = 0, \quad \hat{\phi}_m^k = 0, \quad 1 \le k \le m-2 \tag{27}$$

where $s = a+b+c$. Eqn (27) must be satisfied for any eigenvector ϕ^k. Therefore, it follows that

$$w^k - 1 = \frac{w^k \lambda^k}{s}, \quad s + \left[\frac{ab}{s}\left(\frac{\hat{\lambda}_1^k}{g} - 2\right) - \frac{a^2+b^2}{s} \right] w^k = \lambda^k, \quad 1 \le k \le m-2 \tag{28}$$

Solving Eqn (28) yields

$$w^k = \pm \frac{s}{a+b} \frac{1}{\sqrt{1 - q\left[\sin\frac{k\pi}{2(m-1)} \right]^2}}$$

$$\lambda^k = (a+b)\left\{ 1 - \sqrt{1 - q\left[\sin\frac{k\pi}{2(m-1)} \right]^2} \right\} + c, \quad 1 \le k \le m-2 \tag{29}$$

where

$$q = \frac{4ab}{(a+b)^2} = \frac{4d_1d_2}{(d_1+d_2)^2}, \quad 0 < q \leq 1, \quad d_1 = \alpha K_1, \quad d_2 = (1-\alpha)K_2 \tag{30}$$

Next, we solve for the $m-2$ largest eigenpairs $(\lambda^{r-k}, \phi^{r-k})$, where $r = 2(m-1)$, $1 \leq k \leq m-2$. Assuming that the eigenvectors of the source grid are related to the eigenvectors of the coarse model by

$$\phi_i^{r-k} = -\hat{\phi}_i^k, \quad 1 \leq i \leq m$$

$$\phi_{i,(i+1)}^{r-k} = v^k \hat{\phi}_{i,(i+1)}^k, \quad 1 \leq i \leq m-1, \quad 1 \leq k \leq m-2 \tag{31}$$

yields

$$v^k = w^k, \quad \lambda^{r-k} = (a+b)\left\{ 1 + \sqrt{1 - q\left[\sin\frac{k\pi}{2(m-1)}\right]^2} \right\} + c, \quad 1 \leq k \leq m-2 \tag{32}$$

The middle eigenpair $(\lambda^{m-1}, \phi^{m-1})$ follows directly from the eigenvalue problem (23) and the symmetry condition

$$\lambda^{m-1} = a+b+c = s, \quad \phi_i^{m-1} = 0, \quad 1 \leq i \leq m$$

$$\phi_{i,(i+1)}^{m-1} = -\frac{b}{a}\phi_{(i-1),i}^{m-1} = -\frac{d_2}{d_1}\phi_{(i-1),i}^{m-1}, \quad 2 \leq i \leq m-1 \tag{33}$$

2.1.3 Evaluation of the spectral radius of the two-level iteration matrix

Applying the coarse-model correction iteration matrix T to the eigenvectors of the equivalent stiffness matrix of the source grid yields

$$T\phi^p = (I - Q\bar{K}_0^{-1}Q^T\bar{K})\phi^p, \quad 1 \leq p \leq n-2 \tag{34}$$

where

$$\bar{K}\phi^k = \lambda^k\phi^k, \quad \bar{K}\phi^{r-k} = \lambda^{r-k}\phi^{r-k}, \quad r = 2(m-1)$$

$$\bar{K}\phi^{m-1} = \lambda^{m-1}\phi^{m-1}, \quad 1 \leq k \leq m-2 \tag{35}$$

Based on the prolongation operator (13) and the relationship between the eigenvectors in the source and coarse grids (25) and (31) as well as the source grid eigenvalue problem (26), the restriction of the eigenvectors is given by

$$[\boldsymbol{Q}^T\phi^k]_i = \frac{\lambda^{r-k}}{s}\hat{\phi}_i^k, \quad [\boldsymbol{Q}^T\phi^{r-k}]_i = -\frac{\lambda^k}{s}\hat{\phi}_i^k, \quad r = 2(m-1), \quad 1 \le k \le m-2$$

$$[\boldsymbol{Q}^T\phi^{m-1}]_i = 0, \quad 1 \le i \le m \tag{36}$$

Combining Eqns (35) and (36), and using (17) for the eigenpairs in the coarse grid, yields

$$\boldsymbol{Q}^T\overline{\boldsymbol{K}}\phi^k = \frac{\lambda^k\lambda^{r-k}}{s}\hat{\phi}^k, \quad \boldsymbol{Q}^T\overline{\boldsymbol{K}}\phi^{r-k} = -\frac{\lambda^k\lambda^{r-k}}{s}\hat{\phi}^k, \quad \boldsymbol{Q}^T\overline{\boldsymbol{K}}\phi^{m-1} = 0 \tag{37}$$

$$\overline{\boldsymbol{K}}_0^{-1}\boldsymbol{Q}^T\overline{\boldsymbol{K}}\phi^k = \frac{\lambda^k\lambda^{r-k}}{s\hat{\lambda}^k}\hat{\phi}^k, \quad \overline{\boldsymbol{K}}_0^{-1}\boldsymbol{Q}^T\overline{\boldsymbol{K}}\phi^{r-k} = -\frac{\lambda^k\lambda^{r-k}}{s\hat{\lambda}^k}\hat{\phi}^k, \quad \overline{\boldsymbol{K}}_0^{-1}\boldsymbol{Q}^T\overline{\boldsymbol{K}}\phi^{m-1} = 0 \tag{38}$$

The prolongation of the eigenvectors in the coarse grid based on the operator (13) can be written as

$$[\boldsymbol{Q}\hat{\phi}^k]_{i,(i+1)} = \theta\hat{\phi}_i^k + \delta\hat{\phi}_{i+1}^k = \hat{\phi}_{i,(i+1)}^k = \frac{1}{w^k}\phi_{i,(i+1)}^k = \frac{1}{w^k}\phi_{i,(i+1)}^{r-k}, \quad 1 \le i \le m-1$$

$$[\boldsymbol{Q}\hat{\phi}^k]_i = \hat{\phi}_i^k = \phi_i^k = -\phi_i^{r-k}, \quad 1 \le i \le m, \quad 1 \le k \le m-2 \tag{39}$$

Combining Eqns (34), (38) and (39) yields

$$[\boldsymbol{T}\phi^k]_{i,(i+1)} = \left[1 - \frac{\lambda^k\lambda^{r-k}}{w^k\hat{\lambda}^k s}\right]\phi_{i,(i+1)}^k, \quad [\boldsymbol{T}\phi^k]_i = \left[1 - \frac{\lambda^k\lambda^{r-k}}{\hat{\lambda}^k s}\right]\phi_i^k \tag{40}$$

$$[\boldsymbol{T}\phi^{r-k}]_{i,(i+1)} = \left[1 + \frac{\lambda^k\lambda^{r-k}}{w^k\hat{\lambda}^k s}\right]\phi_{i,(i+1)}^{r-k}, \quad [\boldsymbol{T}\phi^{r-k}]_i = \left[1 - \frac{\lambda^k\lambda^{r-k}}{\hat{\lambda}^k s}\right]\phi_i^{r-k} \tag{41}$$

$$\boldsymbol{T}\phi^{m-1} = \phi^{m-1} \tag{42}$$

Since

$$\phi_{i,(i+1)}^k = \phi_{i,(i+1)}^{r-k}, \quad \phi_i^k = -\phi_i^{r-k}, \tag{43}$$

we can express $\boldsymbol{T}\phi^k$ as

$$\boldsymbol{T}\phi^k = k_1\phi^k + k_2\phi^{r-k} \tag{44}$$

where k_1 and k_2 follow from Eqns (40), (43) and (44)

$$k_1 + k_2 = 1 - \frac{\lambda^k \lambda^{r-k}}{w^k \hat{\lambda}^k s}, \qquad k_1 - k_2 = 1 - \frac{\lambda^k \lambda^{r-k}}{\hat{\lambda}^k s} \tag{45}$$

Solving Eqn (45) yields

$$k_1 = 1 - \frac{w^k + 1}{2w^k} \frac{\lambda^k \lambda^{r-k}}{\hat{\lambda}^k s}, \qquad k_2 = \frac{w^k - 1}{2w^k} \frac{\lambda^k \lambda^{r-k}}{\hat{\lambda}^k s} \tag{46}$$

Likewise, we can express $T\phi^{r-k}$ as

$$T\phi^{r-k} = k_3 \phi^k + k_4 \phi^{r-k} \tag{47}$$

where k_3 and k_4 follow from Eqns (41), (43) and (47)

$$k_3 = \frac{w^k + 1}{2w^k} \frac{\lambda^k \lambda^{r-k}}{\hat{\lambda}^k s}, \qquad k_4 = 1 - \frac{w^k - 1}{2w^k} \frac{\lambda^k \lambda^{r-k}}{\hat{\lambda}^k s} \tag{48}$$

Substituting Eqns (46) and (48) into (44) and (47) yields

$$T\phi^k = (1 - a_1)\phi^k + a_2 \phi^{r-k}, \quad T\phi^{r-k} = a_1 \phi^k + (1 - a_2)\phi^{r-k}, \quad 1 \le k \le m - 2 \tag{49}$$

where

$$a_1 = \frac{w^k + 1}{2w^k} \frac{\lambda^k \lambda^{r-k}}{\hat{\lambda}^k s}, \qquad a_2 = \frac{w^k - 1}{2w^k} \frac{\lambda^k \lambda^{r-k}}{\hat{\lambda}^k s} \tag{50}$$

For simplicity, we consider a two-level cycle with one weighted Jacobi post-smoothing iteration and coarse-level correction. The iteration matrix of the two-level cycle becomes

$$L = ST \tag{51}$$

where

$$S = I - \frac{\omega}{s} \bar{K}, \quad s = a + b + c \tag{52}$$

with ω being the weighting factor of the Jacobi method.

Let the eigenpairs of this two-level iteration matrix L be (Ψ^k, γ^k), $(\Psi^{r-k}, \gamma^{r-k})$ and $(\Psi^{m-1}, \gamma^{m-1})$, where $r = 2(m-1)$ and $1 \le k \le m - 2$, then we have

$$L\Psi^k = \gamma^k \Psi^k, \quad L\Psi^{r-k} = \gamma^{r-k} \Psi^{r-k}, \quad L\Psi^{m-1} = \gamma^{m-1} \Psi^{m-1} \tag{53}$$

From Eqns (42), (52) and (33) it follows that

$$\boldsymbol{L}\phi^{m-1} = \boldsymbol{ST}\phi^{m-1} = \boldsymbol{S}\phi^{m-1} = \left(1 - \frac{\omega}{s}\lambda^{m-1}\right)\phi^{m-1} = (1-\omega)\phi^{m-1} \tag{54}$$

Therefore, we have

$$\Psi^{m-1} = \phi^{m-1}, \quad \gamma^{m-1} = 1-\omega \tag{55}$$

Let Ψ^k be expressed as a linear combination of ϕ^k and ϕ^{r-k}, i.e.,

$$\Psi^k = f_1\phi^k + f_2\phi^{r-k} \tag{56}$$

Then by exploiting the relations

$$\boldsymbol{S}\phi^k = \left(1 - \frac{\omega}{s}\lambda^k\right)\phi^k, \quad \boldsymbol{S}\phi^{r-k} = \left(1 - \frac{\omega}{s}\lambda^{r-k}\right)\phi^{r-k} \tag{57}$$

and using Eqn (49), we have

$$\boldsymbol{L}\Psi^k = \left\{[f_1(1-a_1) + f_2 a_1]\left(1 - \frac{\omega}{s}\lambda^k\right)\right\}\phi^k + \left\{[f_1 a_2 + f_2(1-a_2)]\left(1 - \frac{\omega}{s}\lambda^{r-k}\right)\right\}\phi^{r-k}$$

$$= \gamma^k(f_1\phi^k + f_2\phi^{r-k})$$

from where it follows that

$$[f_1(1-a_1) + f_2 a_1]\left(1 - \frac{\omega}{s}\lambda^k\right) = f_1\gamma^k$$

$$[f_1 a_2 + f_2(1-a_2)]\left(1 - \frac{\omega}{s}\lambda^{r-k}\right) = f_2\gamma^k \tag{58}$$

From the first of the above equations, it follows

$$\gamma^k = \left[(1-a_1) + \frac{f_2}{f_1}a_1\right]\left(1 - \frac{\omega}{s}\lambda^k\right) \tag{59}$$

Let

$$f_1 = a_1\left(1 - \frac{\omega}{s}\lambda^k\right) \tag{60}$$

then, we have

$$\gamma^k = (1 - a_1)\left(1 - \frac{\omega}{s}\lambda^k\right) + f_2 \tag{61}$$

The equation for f_2 is obtained by eliminating γ^k from the second equation in (58) and Eqn (59), and inserting (60) into the resulting equation, which yields

$$f_2^2 + \left\{(1 - a_1)\left(1 - \frac{\omega}{s}\lambda^k\right) - (1 - a_2)\left(1 - \frac{\omega}{s}\lambda^{r-k}\right)\right\}f_2 -$$

$$a_1 a_2\left(1 - \frac{\omega}{s}\lambda^k\right)\left(1 - \frac{\omega}{s}\lambda^{r-k}\right) = 0 \tag{62}$$

The solution of the above quadratic equation is given by

$$(f_2)_{1,2} = \frac{2\tilde{K}(1 - 2\omega)\sqrt{1 - q\chi}}{4\tilde{K} + hqc} \pm$$

$$\frac{16\tilde{K}^2(1 - 2\omega + \omega q\chi) + hqc(1 - \omega)(8\tilde{K} + hqc)}{2(4\tilde{K} + hqc)^2} \tag{63}$$

where

$$\tilde{K} = E_0 A, \quad \chi = \left[\sin\frac{k\pi}{2(m-1)}\right]^2, \quad 1 \leq k \leq m - 2 \tag{64}$$

Likewise, let Ψ^{r-k} be expressed as a linear combination of ϕ^k and ϕ^{r-k}, i.e.,

$$\Psi^{r-k} = f_3\phi^k + f_4\phi^{r-k} \tag{65}$$

where f_3 and f_4 are coefficients which can be determined using similar procedures as described before. Finally, we have

$$\gamma^k = (1 - a_1)\left(1 - \frac{\omega}{s}\lambda^k\right) + (f_2)_1, \quad \gamma^{r-k} = (1 - a_1)\left(1 - \frac{\omega}{s}\lambda^k\right) + (f_2)_2 \tag{66}$$

Inserting Eqn (63) into (66) and accounting for (55) gives the spectrum of the eigenvalues of the two-level iteration matrix

$$\gamma^k = \frac{16\tilde{K}^2(1 - 2\omega + \omega q\chi) + hqc(1 - \omega)(8\tilde{K} + hqc)}{(4\tilde{K} + hqc)^2}$$

$$\gamma^{r-k} = 0, \quad \gamma^{m-1} = 1 - \omega, \quad r = 2(m-1), \quad 1 \le k \le m-2 \tag{67}$$

The spectral radius of the two-level iteration matrix $\rho(L)$ is defined as the largest absolute value of the eigenvalues of L:

$$\rho(L) = \max\{|\gamma^k|, 1 - \omega\} \tag{68}$$

Since $0 \le \chi \le 1$, the weighting factor for the Jacobi method is chosen to provide the same rate of convergence for the two extreme values:

$$|\gamma^k|_{(\chi = 0)} = |\gamma^k|_{(\chi = 1)} \tag{69}$$

Inserting the first expression in (67) into (69) gives

$$\omega = \frac{16\tilde{K}^2 + hqc(8\tilde{K} + hqc)}{(32 - 8q)\tilde{K}^2 + hqc(8\tilde{K} + hqc)} \tag{70}$$

It can be seen that $0 < \omega < 1$ since $0 < q \le 1$ and both the numerator and the denominator of (70) are positive with the denominator greater than the numerator.
Substituting (70) into the first expression of (67) yields

$$\max(|\gamma^k|) = \frac{q}{4 - q + 2\kappa(2 + \kappa)}, \quad \kappa = \frac{c}{a + b} \tag{71}$$

where the following relations have been exploited

$$q = \frac{4ab}{(a+b)^2}, \quad \frac{\tilde{K}}{h} = \frac{ab}{a+b}, \quad \frac{\tilde{K}}{hqc} = \frac{a+b}{4c} \tag{72}$$

For the case of $\alpha = 0.5$ and $\rho_1 = \rho_2$, Eqn (71) can be written in the form

$$\max(|\gamma^k|) = \frac{1}{1 + d + \dfrac{1}{d} + 4\zeta^2[d(1 + 2\zeta^2) + 1]} \tag{73}$$

where $d \ge 1$ is the ratio of micro-constituent elastic moduli and ζ is the ratio between the critical time step (i.e., the time for a wave to propagate through a single element) and the time step size employed for implicit time integration

$$1 \le d = E_1/E_2, \quad \xi = \Delta t_{cr}/\Delta t \tag{74}$$

Remark 1: d and ζ in (73) are two non-dimensional parameters which characterize the degree of material heterogeneity and system dynamics, respectively. $\xi = 0$ corresponds

to the static case, in which case we recover the rate of convergence, $(1 + d + 1/d)^{-1}$, pre-viously obtained by the first author [33]. For $\xi = 0$ and a homogeneous medium, $d = 1$, with the volume fraction $\alpha = 0.5$, Eqn (71) gives $\rho^* = 1/3$, which corresponds to the classical multigrid method.

Remark 2: The mid-frequency eigenvector corresponding to the eigenvalue $(1 - \omega)$ is ϕ^{m-1} (see Eqn (33)). This mid-frequency mode of error can be filtered out using global basis method [35][36] as described by Eqn. (2) and the resulting rate of convergence is then governed by (71) and (73).

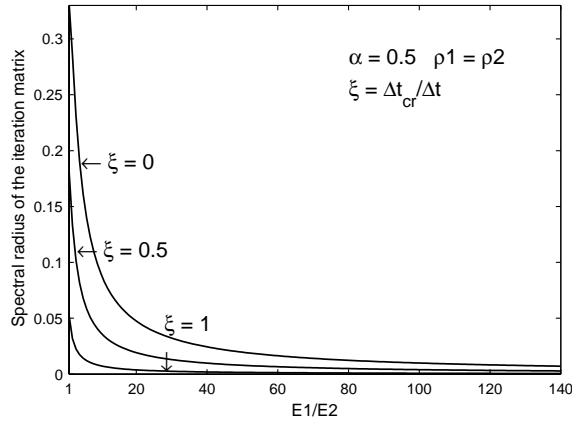The plot of spectral radius of the two-level iteration matrix (73) is given in Figure 7.

Figure 7: The rate of convergence of the two-level method

2.2 Convergence of the RVE based aggregation method

Enforcing compatibility between adjacent RVEs is trivial for one-dimensional prob-lems only. In multi-dimensions, however, it is more convenient to employ an aggregation approach, which does not require compatibility between adjacent aggregates or RVEs in the present context [9][10][11][12]. Instead, an interface of one layer of "soft" elements is formed between the aggregates. The rate of convergence of the aggregation method is governed by the spectral radius of the interface elements stiffness matrix and the cut-off eigenvalue below which all the aggregate modes are included in the coarse model.

For the model problem under consideration it is convenient to define a three-element RVE as shown in Figure 8. Between two adjacent RVEs there is a "soft" interface element ($E_2 \leq E_1$). As before, we denote the number of nodes in the coarse grid by *m*. The number
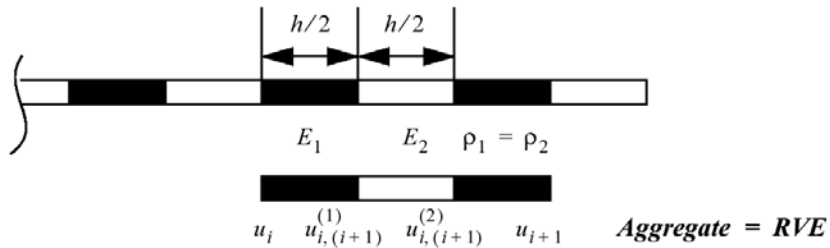

Figure 8: Aggregation model in 1D

of nodes in the source grid is $n = 2m$. In the source grid, the nodal displacements at the RVE boundaries are denoted by u_i and the nodal displacements inside the RVE are denoted as $u_{i,(i+1)}^{(1)}$ and $u_{i,(i+1)}^{(2)}$. We seek to estimate numerically the rate of convergence of the RVE based aggregation method. For simplicity, attention is restricted to the case of constant mass density, $\rho_1 = \rho_2$, and the volume fraction $\alpha = 0.5$.

2.2.1 The prolongation operator
The equivalent stiffness matrix for the three-element aggregate is given by

$$\overline{K}_a = \begin{bmatrix} a + c/2 & -a & 0 & 0 \\ -a & a + b + c & -b & 0 \\ 0 & -b & a + b + c & -a \\ & & -a & a + c/2 \end{bmatrix} \tag{75}$$

The prolongation operator for a single aggregate is constructed based on the constrained minimization problem:

$$\Pi_a = \frac{1}{2}\phi^T \overline{K}_a \phi, \quad \text{subjected to } \|\phi\|_2 = 1 \tag{76}$$

where

$$\phi = \begin{bmatrix} u_i & u_{i,(i+1)}^{(1)} & u_{i,(i+1)}^{(2)} & u_{i+1} \end{bmatrix}^T \tag{77}$$

which yields the following eigenvalue problem:

$$\overline{K}_a \phi = \lambda_a \phi, \quad \|\phi\|_2 = 1 \tag{78}$$

The prolongation matrix of the aggregate takes the following form:

$$\begin{bmatrix} q_1 & q_2 \end{bmatrix} \begin{bmatrix} \hat{u}_i \\ \hat{u}_{i+1} \end{bmatrix} = \phi, \quad 1 \le i \le m - 1 \tag{79}$$

where $q_1 = \begin{bmatrix} \theta_1 & \theta_2 & \theta_3 & \theta_4 \end{bmatrix}^T$ and $q_2 = \begin{bmatrix} \delta_1 & \delta_2 & \delta_3 & \delta_4 \end{bmatrix}^T$ are the eigenvectors corresponding to the first two smallest eigenvalues of the eigenvalue problem (78).

The global prolongation operator $\tilde{Q}$ is formed by assembling the prolongation matrices of each aggregate, which yields:

$$\tilde{Q} = \begin{bmatrix} q_1 & q_2 & & & \\ & & q_1 & q_2 & \\ \cdots & \cdots & \cdots & \cdots & \\ & & & & q_1 & q_2 \end{bmatrix}_{n \times m} \tag{80}$$

2.2.2 The spectral radius of the two-level iteration matrix

The coarse-model equivalent stiffness matrix is formed by restriction of the source grid matrix, i.e. $\bar{K}_0 = \tilde{Q}^T \bar{K} \tilde{Q}$. We consider the two-level iteration process consisting of three SSOR *(Symmetric Successive Overrelaxation Method)* pre- and post- smoothing iterations. The spectral radius of the two-level iteration matrix $\rho(S^3 T S^3)$ is evaluated numerically and the results are presented in Table 1.

It can be seen that the RVE based aggregation method has similar convergence characteristics observed in the RVE based two-level method, i.e., the rate of convergence increases with increasing material heterogeneity and decreasing time integration step. For both static and dynamic cases, the rate of convergence is independent of the size of the problem.

TABLE 1. Spectral radius of the RVE based aggregation method ($\xi = \Delta t_{cr} / \Delta t$)

$\rho(S^3 T S^3)$	$n = 40$	$n = 80$	$n = 120$	$n = 160$	$n = 200$
$E1/E2 = 1, \xi = 0$	0.0242	0.0242	0.0243	0.0243	0.0243
$E1/E2 = 10, \xi = 0$	0.0450	0.0450	0.0450	0.0450	0.0450
$E1/E2 = 100, \xi = 0$	0.0116	0.0116	0.0116	0.0116	0.0116
$E1/E2 = 1000, \xi = 0$	0.0013	0.0013	0.0013	0.0013	0.0013
$E1/E2 = 1, \xi = 0.5$	1.36×10^{-5}	1.36×10^{-5}	1.36×10^{-5}	1.36×10^{-5}	1.36×10^{-5}
$E1/E2 = 10, \xi = 0.71$	2.06×10^{-6}	2.06×10^{-6}	2.06×10^{-6}	2.06×10^{-6}	2.06×10^{-6}
$E1/E2 = 100, \xi = 0.16$	0.0234	0.0234	0.0234	0.0234	0.0234
$E1/E2 = 1000, \xi = 0.5$	1.86×10^{-4}	1.86×10^{-4}	1.86×10^{-4}	1.86×10^{-4}	1.86×10^{-4}

3.0 Convergence for 2D model problem

We consider a 2D structured mesh and restrict our attention to the static case. The problem configuration and the spatial discretization scheme are shown in Figure 9. The RVE consists of 9 elements totaling 32 degrees of freedom as illustrated in Figure 9.
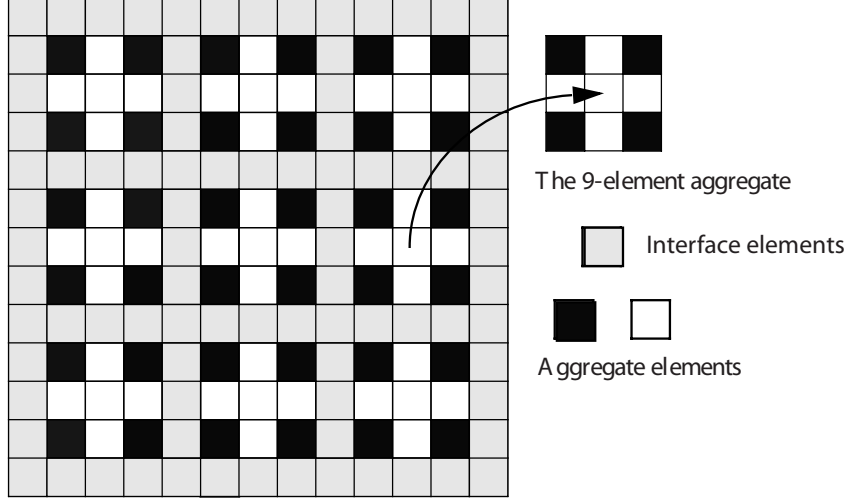

Figure 9: Aggregation model in 2D

As in 1D case, the global prolongation operator $\tilde{Q}$ is a block diagonal matrix formed by assembling the prolongation matrices of each aggregate:

$$\tilde{Q} = \mathrm{diag}\{\tilde{Q}_a, \tilde{Q}_a, ..., \tilde{Q}_a\} \tag{81}$$

where the prolongation matrix of the aggregate $\tilde{Q}_a$ is obtained from the solution of the eigenvalue problem:

$$K_a \phi = \lambda_a \phi \tag{82}$$

with K_a being the stiffness matrix of the aggregate. Eigenvectors corresponding to the $N^{inc} \cdot N^{rbd}$ smallest eigenvalues of K_a are chosen for the construction of $\tilde{Q}_a$, where N^{inc}, N^{rbd} are the number of inclusions and rigid body modes per inclusion in the RVE. In the present case: $N^{inc} = 4, N^{rbd} = 3$.

As in 1D case, we consider a two-level iterative process consisting of three SSOR pre- and post- smoothing iterations. The spectral radius of the two-level iteration matrix $\rho(S^3 T S^3)$ is evaluated numerically and the results are given in Table 2.

TABLE 2. Spectral radius for a single multilevel cycle (2D 9-element RVE), statics

$\rho(S^3 T S^3)$	$n = 18 \times 18$	$n = 22 \times 22$	$n = 30 \times 30$
E1/E2 = 1	0.1157	0.1441	0.1820
E1/E2 = 10	0.0610	0.0628	0.0650

TABLE 2. Spectral radius for a single multilevel cycle (2D 9-element RVE), statics

$E1/E2 = 100$	0.0260	0.0261	0.0262
$E1/E2 = 1000$	0.0037	0.0037	0.0037

4.0 Comparison of solvers and discussion

Numerical results of the RVE-based methods are compared to those of the classical con-jugate gradient and two-grid methods for 1D model problem defined in Figure 6. One end of the problem domain in Figure 6 is fixed, while the other end is subjected to a load P. For the statics, $P = P_0$, where $P_0 = 50$ KN. For dynamics, $P = P_0 \sin(\omega t)$, if $0 \le t \le \pi/\omega$

and $P = 0$, if $t > \pi/\omega$, where the frequency of the excitation is $\omega = 3 \times 10^4$.

For all multi-level solvers (MG), we take three SSOR pre- and post- smoothing itera-tions. For the PCG *(Preconditioned Conjugate Gradient)* solver, the SSOR preconditioner is employed. The stopping criterion is taken as

$$\frac{\|r\|_2}{\|f\|_2} \le \eta = 10^{-8} \tag{83}$$

where $\| \ \|_2$ is the 2-norm.

TABLE 3. Number of iterations for the two-element RVE, statics ($\eta = 10^{-8}$)

Source Mesh Size		n=402				n=1002		
E1/E2	1	10	100	1000	1	10	100	1000
RVE based MG	10	7	6	4	10	7	5	4
Classical MG	10	44	435	4344	10	44	436	4358
PCG	156	227	268	286	364	541	662	711

TABLE 4. Number of iterations for the two-element RVE, dynamics, n=1002 ($\eta = 10^{-8}$)

	Solvers	RVE based MG	Classical MG	PCG
$E1/E2 = 1$	$\Delta t_{cr}/\Delta t_1 = 0.45$	2	2	8
	$\Delta t_{cr}/\Delta t_3 = 0.90$	1	1	4
$E1/E2 = 10$	$\Delta t_{cr}/\Delta t_1 = 0.19$	5	6	15
	$\Delta t_{cr}/\Delta t_2 = 0.39$	3	3	9
	$\Delta t_{cr}/\Delta t_3 = 0.96$	1	1	5
$E1/E2 = 100$	$\Delta t_{cr}/\Delta t_1 = 0.06$	4	60	21
	$\Delta t_{cr}/\Delta t_2 = 0.25$	2	6	8
	$\Delta t_{cr}/\Delta t_3 = 0.97$	1	1	4
$E1/E2 = 1000$	$\Delta t_{cr}/\Delta t_1 = 0.02$	4	702	22
	$\Delta t_{cr}/\Delta t_2 = 0.20$	2	14	6
	$\Delta t_{cr}/\Delta t_3 = 0.98$	1	1	3

Results for the two-element RVE model are presented in Table 3 for statics and in Table 4 for dynamics. The corresponding results for the three-element RVE model are presented in Table 5 and Table 6, respectively.

It can be observed that in statics, the rate of convergence for both the classical multigrid and the PCG solvers deteriorates rapidly as the degree of material heterogeneity increases, while the rate of convergence for the RVE based multigrid solver improves. The rate of convergence for both the RVE and the classical multigrid solvers is independent of the mesh refinement. However, the rate of convergence for the PCG solver deteriorates rapidly as the problem size increases.

TABLE 5. Number of iterations for the 3-element RVE, statics ($\eta = 10^{-8}$)

Source Mesh Size	n=1001				n=2001			
E1/E2	1	10	100	1000	1	10	100	1000
Aggregation	5	5	5	4	5	5	5	4
Classic MG	8	18	136	1271	8	18	139	1561
PCG	364	526	601	622	705	1030	1194	1250

TABLE 6. Number of iterations for the 3-element RVE, dynamics, n=2001 ($\eta = 10^{-8}$)

	Solvers	RVE based Aggregation	Classic MG	PCG
E1/E2 = 1	$\Delta t_{cr}/\Delta t_1 = 0.23$	3	3	15
	$\Delta t_{cr}/\Delta t_2 = 0.45$	2	2	8
	$\Delta t_{cr}/\Delta t_3 = 0.90$	1	1	5
E1/E2 = 10	$\Delta t_{cr}/\Delta t_1 = 0.08$	4	8	27
	$\Delta t_{cr}/\Delta t_2 = 0.16$	4	6	15
	$\Delta t_{cr}/\Delta t_3 = 0.82$	1	2	4
E1/E2 = 100	$\Delta t_{cr}/\Delta t_1 = 0.03$	4	52	34
	$\Delta t_{cr}/\Delta t_2 = 0.26$	4	6	6
	$\Delta t_{cr}/\Delta t_3 = 0.87$	1	2	4
E1/E2 = 1000	$\Delta t_{cr}/\Delta t_1 = 0.008$	4	910	34
	$\Delta t_{cr}/\Delta t_2 = 0.08$	4	42	8
	$\Delta t_{cr}/\Delta t_3 = 0.83$	1	2	4

In dynamics, if the time step is close to critical, all solvers converge rapidly. This is due to the fact that the equivalent stiffness matrix is dominated by the diagonal mass matrix. For larger time steps and in the case of high degree of material heterogeneity, the classical multigrid solver might underperform PCG solver due to poor choice of the coarse grid space. On the other hand, the RVE based solvers converge rapidly for all cases considered.

5.0 Summary and conclusions

A dedicated multilevel method for wave propagation problems in periodic heterogeneous media is developed and validated. The intergrid transfer operators are constructed from the solution of the Representative Volume Element (RVE) problem. The rate of convergence of the RVE-based multilevel has been shown to improve with increasing material heterogeneity or mismatch parameter between the stiffnesses of microconstituents and decreasing time integration step. Numerical results confirm theoretical estimates.

The methodology developed will find its use in practical applications where the homogenization theory in not applicable due to the fact that the size of the microstructure is comparable in magnitude to that of structural details or the wavelength of a traveling signal. This class of problems falls into the grey area where the structural and material systems cannot be separated. Among the applications falling into this category are: woven architectures in aircraft engines, airframes, tires, micro-electronic devices, and porous engineering materials such as honeycombs and truss-like materials. Many of these applications are characterized by strong mismatch of microconstituents stiffnesses resulting in rapid convergence of the RVE-based multilevel process.

Acknowledgment

References

1   Fish J., Yu Q., and Wildman D., Simulation of progressive damage for high temperature woven composites. *Proceedings of American Ceramic Society.* Cocoa Beach meeting, Jan 12-16, 1999.

2   Fish, J., LeMonds, and Shek K., Modeling and simulation of wrinkling in compression molding process of fiber reinforced composites. *Journal of Engineering Mechanics*, 1999; **125(**8): 951-955.

3   Ebbott TG., An application of finite element based fracture mechanics analysis to cord/rubber structures. *The 12th Annual Meeting of The Tire Society.* The University of Akron, OH, 1993.

4   Ebbott TG., Hohman RL., Jeusette JP. and Kerchman V., Tire temperature and rolling resistance prediction with finite element analysis. *The 15th Annual Meeting of The Tire Society.* The University of Akron, OH, 1996.

5   Tummala RR. and Rymaszewski EJ., Microelectronics Packaging Handbook. Van Nostrand Reinhold, New York, 1989.

6   JAMCORP, 17 Jonspin Rd.,Wilmington, MA 01887-1020, US. http://www.jam-corp.com/brochure/brocperf.htm.

7   Fish J., Yu Q., and Shek KL., Computational damage mechanics for composite materials based on mathematical homogenization. *International Journal for Numerical Methods in Engineering,* 1999; **45:**1657-1679.

8   Wentorf R., Shephard MS., Dvorak GJ., Fish J., Beall MW., Collar R., Shek K., Software framework for mechanism-based design of composite structures. *Proceedings of American Ceramic Society.* Cocoa Beach meeting, Jan 12-16, 1997.

9   Fish J. and Belsky V., Generalized aggregation multilevel solver. *International Journal for Numerical Methods in Engineering*, 1997; **40:** 4341-4361.

10   Fish J. and Suvorov A., Automated adaptive multilevel solver. *Comp. Meth. Appl. Mech. Engng.*, 1997; **149:** 267-287.

11   Fish J., Suvorov A., and Qu Y., Towards robust two-level methods for indefinite systems. *International Journal for Numerical Methods in Engineering,* 1999; **45:** 1433-1456.

12   Fish J., and Korneev V., On two-level methods based on aggregation for 3D problems. submitted to *Comp. Meth. Appl. Mech. Engng.*, (1999).

13   Fish J., Nayak P., Holmes MH., Microscale reduction error indicators and estimators for a periodic heterogeneous medium. *Computational Mechanics*, 1994; **14:** 323-338.

14   Fish J., and Markolefas S., Guttal R. and Nayak P., On adaptive multilevel superposition of finite element meshes. *Applied Numerical Mathematics,* 1994; **14:** 135-164.

15   Ghosh S. and Mukhopadhyay AN., A material based finite element analysis of heterogeneous media involving Dirichlet tessellations. *Computer Methods in Applied Mechanics and Engineering*, 1993; **104:** 211-247.

16   Lee KH., Moorthy S. and Ghosh S., Asymptotic homogenization with microstructural VCFEM for modeling heterogeneous materials. *Proceedings of the* 3rd *US congress on computational mechanics*, Texas, 1995.

17   Lissenden CJ. and Herakovich CT., Numerical modeling of damage development in viscoplasticity and metal matrix composites. *Computer Methods in Applied Mechanics and Engineering*, 1995; **126:** 289-303.

18   Holister SJ. and Kikuchi N., A comparison of homogenization and standard analyses for periodic porous composites. *Computational Mechanics*, 1992; **10:** 73-95.

19   Guedes JS. and Kikuchi N., Preprocessing and postprocessing for materials based on the homogenization method with adaptive finite element methods. *Computer Methods in Applied Mechanics and Engineering*, 1989; **83:** 143-198.

20   Fish J., and Wagiman A., Multiscale finite element method for a locally nonperiodic heterogeneous medium. *Computational Mechanics*, 1993; **12:** 164-181.

21   Fish J., Shek K., Pandheeradi M. and Shephard MS, Computational plasticity for composite structures based on mathematical homogenization: Theory and practice, *Computer Methods in Applied Mechanics and Engineering*, 1997; **148:** 53-73.

22   Belytschko T., Fish J. and Bayliss A., The spectral overlay on the finite element solutions with high gradients. *Computer Methods in Applied Mechanics and Engineering*, 1990; **81:** 71-89.

23   Fish J., The s-version of the finite element method. *SCOREC report 90-18*, 1990; *Computers and Structures*, 1992; **43:** 539-547.

24   Fish J., Hierarchical modeling of discontinuous fields. *Communications in Applied Numerical Methods*, 1992; **8:** 443-453.

25   Fish J. and Markolefas S., The s-version of the finite element method for multilayer

laminates. *International Journal for Numerical Methods in Engineering*, 1992; **33:** 1081-1105.

26 Fish J. and Markolefas S., Adaptive s-method for linear elastostatics. *Computer Methods in Applied Mechanics and Engineering*, 1993; **103:** 363-396.

27 Fish J. and Guttal R., The s-version of finite element method for laminated composites. *International Journal for Numerical Methods in Engineering*, 1996; **39:** 3641-3662.

28 Rank E. and Krause R., A multiscale finite element method. *Numerische Methoden und Informationsverarbeitung report, 165-1995*, University of Dortmund, Germany, 1995.

29 Stanley G., Levit I., Stehlin B. and Hurlbut B., Adaptive finite element strategies for shell structures. The *33rd AIAA/ASME Structure, Structural Dynamics and Materials Conference*, Dallas, 1992.

30 Piltner, Special finite elements with holes and internal cracks. *International Journal for Numerical Methods in Engineering*, 1985; **21:** 1471-1485.

31 Noor AK., Burton WS. and Peters JM, Hierarchical Adaptive Modeling of Structural Sandwiches and Multilayered Composite Panels. *Applied Numerical Mathematics*, 1994; **14**.

32 Fish J. and Markolefas S., Adaptive global-local refinement strategy based on the interior error estimates of the h-method. *International Journal for Numerical Methods in Engineering*, 1994; **37:** 827-838.

33 Fish J. and Belsky V., Multigrid method for a periodic heterogeneous medium. Part I: Convergence studies for one-dimensional case. *Comp. Meth. Appl. Mech. Engng.*, 1995; **126:** 1-16.

34 Fish J. and Belsky V., Multigrid method for a periodic heterogeneous medium. Part 2: Multiscale modeling and quality control in multidimensional case. *Comp. Meth. Appl. Mech. Engng.*, 1995; **126:** 17-38.

35 Fish J. and Qu Y., Global basis two-level method for indefinite systems. Part 1: convergence studies. *International Journal for Numerical Methods in Engineering*, 2000; **49:** 439-460.

36 Qu Y. and Fish J., Global basis two-level method for indefinite systems. Part 2: Computational issues. *International Journal for Numerical Methods in Engineering*, 2000; **49:** 461-478.

37 Hackbusch W. and Trottenberg U., *Multigrid Methods*. Springer: Berlin, 1992.

38 Hackbusch W., *Iterative Solution of Large Sparse Systems of Equations*. Springer: Berlin, Heidelberg, New York, Tokyo, 1994.

39 Parsons ID. and Hall JF., The multigrid method in solid mechanics: Part 1-algorithm description and behavior. *International Journal for Numerical Methods in Engineering*, 1990; **29:** 719-737.

40   Parsons ID. and Hall JF., The multigrid method in solid mechanics: Part 2-practical applications. *International Journal for Numerical Methods in Engineering*, 1990; **29:** 739-753.

41   Giddings TE. and Fish J., An algebraic two-level preconditioner for asymmetric, positive-definite systems. *International Journal for Numerical Methods in Engineering*, 2001; **52:** 1443-1463.

42   Hughes TJR., *The Finite Element Method, Linear Static and Dynamic Finite Element Analysis*. Prentice-Hall: Englewood Cliffs. NJ, 1987.

43   Fish J. and Chen W., On accuracy, stability and efficiency of the Newmark method with incomplete solution by multilevel methods. *International Journal for Numerical Methods in Engineering*, 1999; **46:** 253-273.

44   Benssousan A., Lions JL. and Papanicoulau G., *Asymptotic Analysis for Periodic Structures*. North Holland: Amsterdam, 1978.

45   Bakhvalov, NS. and Panasenko GP., *Homogenization: Averaging Processes in Periodic Media*. Kluwer: Dordrecht, 1989.

46   Chen W. and Fish J., A dispersive model for wave propagation in periodic heterogeneous media based on homogenization with multiple spatial and temporal scales. *Transactions of the ASME, Journal of Applied Mechanics*, 2001; **68**: 153-161.

47   Barrett R., Berry M., Chan TF., Demmel J., et. al., *Templates for the Solution of Linear Systems: Building Blocks for Iterative Methods*. http://netlib2.cs.utk.edu/linalg/html_templates/Templates.html